J Mater Sci (2007) 42:7135–7140
DOI 10.1007/s10853-007-1569-y

Phase equilibria in the pseudo-binary In_2O_3–SnO_2 system

William J. Heward · Douglas J. Swenson

Received: 22 December 2006 / Accepted: 29 January 2007 / Published online: 5 May 2007

Abstract The pseudo-binary In_2O_3–SnO_2 phase diagram has been determined in the range of 1000–1650 °C using electron probe microanalysis (EPMA) and x-ray diffraction (XRD) analysis of solid-state sintered samples. The solubility of SnO_2 in In_2O_3 was found to range from 1.3 mol% at 1000 °C to a maximum of 13.1 mol% at 1650 °C, indicating that commercial SnO_2-doped In_2O_3 thin films are thermodynamically metastable. In_2O_3 was found to have negligible solubility in SnO_2 throughout the temperatures examined. In this study two intermediate compounds, $In_4Sn_3O_{12}$ and In_2SnO_5, were found. Each phase was found to be stable only at high temperatures, decomposing eutectoidally at 1325 and 1575 °C, respectively. This is believed to be the first report of the high temperature phase In_2SnO_5, which is attractive for future research as a transparent conducting oxide.

Introduction

Recently, the commercial demand for higher quality optoelectronic components has increased the amount of research in the class of materials known as transparent conducting oxides (TCOs). Due to its combination of high conductivity (~10^3 S cm^{-1}) and high transparency in the visible spectrum (>80%) when in the form of a thin-film, SnO_2-doped In_2O_3, or indium-tin-oxide (ITO), has been the leading TCO material in a variety of optoelectronic applications for the last few decades. Its importance has considerably grown due to its wide use in flat screen display (FSD) devices. Though sputtering of either metallic or oxide targets remains the most common deposition technique to produce ITO films, there has been work focusing on a variety of other methods for depositing ITO films onto glass and polymer substrates [1]. The absence of an equilibrium phase diagram considerably hinders adequate characterization of ITO films with regard to their equilibrium states. This lack of information may impact its use in large output industries where robust metrology techniques must be available to effectively control device quality.

The way in which the solubility of SnO_2 in In_2O_3 behaves as a function of temperature is not well understood. Various solubilities have been reported for a number of isotherms, however oftentimes there is not good agreement among the results [2–10]. In the In_2O_3–SnO_2 system there have been reports of a number of intermediate compounds. $In_4Sn_3O_{12}$ was first reported in 1986 by Bates et al. [2], and has since been well characterized by Naudad et al. [11]. Solov'eva and Zhdanov [3] reported the existence of the pyrochlore compound $In_2Sn_2O_7$ above 1200 °C, however no other authors have confirmed its existence. Varfolomeev et al. [4] reported a low temperature compound with the stoichiometry In_2SnO_5 to form when using thermal decomposition of hydroxides at 1000 °C and above. The Powder Diffraction File (PDF) card for this phase (#32–458) has been deleted from the International Center for Diffraction Data (ICDD) database, and we note the similarities of this card to the high-pressure corundum-type structure of In_2O_3 (#22–336). Enoki et al. [5] reported

W. J. Heward · D. J. Swenson
Department of Materials Science and Engineering, Michigan Technological University, Houghton, MI 49931, USA

Present Address:
W. J. Heward (✉)
Microstructural and Surface Sciences Laboratory, GE Global Research Center, Niskayuna, NY 12309, USA
e-mail: heward@research.ge.com

appreciable solubility of In_2O_3 in SnO_2, however Bates et al. [2], Edwards et al. [6], and Frank et al. [7], reported that the solubility of In_2O_3 in SnO_2 is negligible.

This paper presents an equilibrium In_2O_3–SnO_2 phase diagram in the region of 1000–1650 °C as determined using an electron probe microanalyzer (EPMA) and x-ray diffraction (XRD) analysis. SnO_2 was found to have a maximum solubility of 13.1 mol% in In_2O_3 at 1650 °C. Two line compounds, $In_4Sn_3O_{12}$ and In_2SnO_5, were found to exist in the studied temperature range. We believe this report contains the first unambiguous experimental evidence by x-ray diffraction for the high temperature phase In_2SnO_5, whose composition is confirmed using EMPA. This compound may have potential applications for future industrial use as a transparent conductive oxide.

Experimental

SnO_2 and In_2O_3 powders (>99.999% pure) were used to prepare samples whose compositions are illustrated in Fig. 2. All of the compositions were sintered between 800 °C and 1650 °C. Stoichiometric amounts of the oxides were also mixed to produce samples of In_2SnO_5 and $In_4Sn_3O_{12}$ for the 1600 °C and 1400 °C isotherms, respectively. The mixed powders were pressed into 0.75 inch diameter pellets using an applied load of 468MPa. Samples were placed on an alumina plate, and embedded in mixed oxide of the same composition to help prevent sublimation. Sintering times ranged from 3 h for the 1650 °C samples to 840 h for the 1000 °C and 800 °C samples. The low temperature samples ($\leq$ 1400 °C) were given intermediate grindings, repressed, and reheated. After equilibrating, the samples were air-cooled. A small portion of each sample was ground into a fine powder with a mortar and pestle for XRD analysis. Qualitative phase identification and structural analysis of the phases present in the samples was carried out using a Scintag θ/θ diffractometer using CuK_α radiation. Samples were mounted in back-loading cavity holders and scans were run from 10° to 90° 2θ with a step size of 0.02° and a count time of 2–10 s. SRM 640b silicon powder was used for external theta calibration. The XRD data reported for $In_4Sn_3O_{12}$ and In_2SnO_5 were from samples made on stoichiometry at 1400 °C and 1600 °C, respectively. The fired $In_4Sn_3O_{12}$ and In_2SnO_5 samples contained a small amount of excess In_2O_3, presumably a result of sublimation of SnO_2.

A JEOL JXA-8600 Superprobe Electron Probe Microanalyzer (EPMA) was used to determine the elemental compositions of the phases present in each sample using wavelength dispersive spectrometry (WDS). A beam current of 20nA was generated using an accelerating voltage of 15 kV. The standards used were elemental Sn, and InAs. Results were reported in weight percents of component oxides where the oxygen was calculated by assuming stoichiometry of the reported oxide. The totals were consistently between 98% and 102% total oxides. To determine if a sample had reached thermodynamic equilibrium and was homogeneous, data was collected in at least four locations from each phase at four different single-phase areas in the sample. In addition to this systematic approach of taking readings, approximately five random points were measured on each phase in each sample. In order to avoid spurious readings from neighboring phases, point readings were taken at least 1–2 microns away from phase boundaries. If the quantitative results from the point readings were all very similar, the sample was judged to be in thermodynamic equilibrium. 1σ errors for the compositional results are given in Table 1, and were found to be 0.6 mol% or less. The compositions reported for $In_4Sn_3O_{12}$ are the averages determined from compositional readings recorded from two-phase samples on each side of the phase boundary. Taken separately, these readings were identical or overlapped within the standard deviation, thus only one $In_4Sn_3O_{12}$ composition is reported for each isotherm.

Results and discussion

Phase equilibria

The equilibrium compositions for each phase in the samples of this experiment are listed in Table 1, and the resulting phase diagram is given as Fig. 1. The solvus line between In_2O_3 and SnO_2, $In_4Sn_3O_{12}$, or In_2SnO_5 produced in this study is well behaved, and a considerably more accurate trend line can be drawn when compared with those previously reported [5, 8].

The solid solubility of SnO_2 in In_2O_3 is shown in detail in Fig. 2. This solvus line is similar to that reported by Ohya [8], however, the agreement is varied with other reports [2–4, 6, 7, 9, 10]. It is difficult to comment on discrepancies where they occur for a few reasons. Chief among them is the metastabilty of ITO thin films, as well difficulty in observing intermediate compounds as secondary phases in bulk x-ray studies [10, 12]. Another difficulty, where energy dispersive spectroscopy (EDS) is used, is that huge spectral overlap exists between the In and Sn L-shell families of peaks, making matrix effects significant, and quantification difficult. On a microscopic level, this necessitates WDS in order to quantify the In and Sn levels.

It is unclear whether or not the sample heated at 800 °C reached equilibrium, or if the solubility of SnO_2 in In_2O_3 at this temperature is below the detection limit of the instrument. The average detection limit given for the

Table 1 Equilibrium compositions determined in this study for the In_2O_3–SnO_2 system

Isotherm (°C)	Gross Composition (mol%)		Phases identified by XRD	Composition of phases (mol%, SnO_2)
	In_2O_3	SnO_2		
1650	70	30	In_2O_3, In_2SnO_5	13.1(0.4), 48.3(0.4)
1650	45	55	In_2SnO_5, $In_4Sn_3O_{12}$	50.3(0.2), 60.3(0.4)
1650	30	70	$In_4Sn_3O_{12}$, SnO_2	
1600	70	30	In_2O_3, In_2SnO_5	12.2(0.4), 49.5(0.3)
1600	45	55	In_2SnO_5, $In_4Sn_3O_{12}$	50.2(0.4), 60.5(0.3)
1600	30	70	$In_4Sn_3O_{12}$, SnO_2	99.7(0.1)
1575	70	30	In_2O_3, $In_4Sn_3O_{12}$	11.5(0.3), 58.8(0.6)
1550	70	30	In_2O_3, $In_4Sn_3O_{12}$	10.2(0.3), 60.9(0.3)
1550	30	70	$In_4Sn_3O_{12}$, SnO_2	
1500	70	30	In_2O_3, $In_4Sn_3O_{12}$	8.3(0.3), 59.6(0.3)
1500	30	70	$In_4Sn_3O_{12}$, SnO_2	99.7(0.1)
1450	70	30	In_2O_3, $In_4Sn_3O_{12}$	6.5(0.2), 60.2(0.2)
1450	30	70	$In_4Sn_3O_{12}$, SnO_2	
1400	70	30	In_2O_3, $In_4Sn_3O_{12}$	5.3(0.3), 60.0(0.4)
1400	30	70	$In_4Sn_3O_{12}$, SnO_2	99.7(0.1)
1350	70	30	In_2O_3, $In_4Sn_3O_{12}$	4.5(0.2), 58.9(0.5)
1350	30	70	$In_4Sn_3O_{12}$, SnO_2	
1325	70	30	In_2O_3, SnO_2	4.2(0.3)
1325	30	70	In_2O_3, SnO_2	
1300	70	30	In_2O_3, SnO_2	3.9(0.4), 99.8(0.1)
1300	30	70	In_2O_3, SnO_2	
1200	70	30	In_2O_3, SnO_2	2.8(0.3)
1200	10	90	In_2O_3, SnO_2	
1000	70	30	In_2O_3, SnO_2	1.3(0.3)
1000	10	90	In_2O_3, SnO_2	
800	70	30	In_2O_3, SnO_2	
800	10	90	In_2O_3, SnO_2	

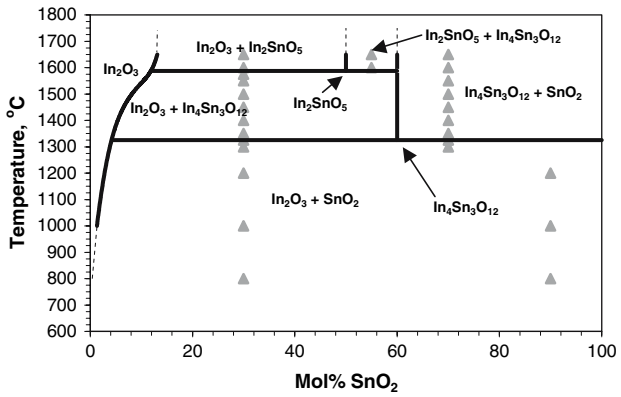

Fig. 1 Phase equilibria in the In_2O_3–SnO_2 system, produced using the compositions listed in Table 1. The solid triangles represent bulk compositions of samples used to obtain compositional data. (The maximum solubility of In_2O_3 in SnO_2 was found to be 0.3 mol%; not shown in the figure)

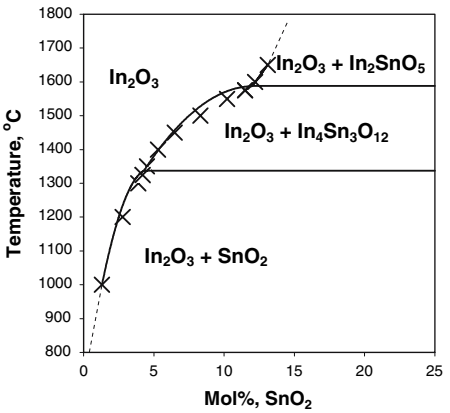

Fig. 2 The In_2O_3 rich side of the In_2O_3–SnO_2 of the phase diagram, showing the solid solubility range of SnO_2 in In_2O_3

readings in this sample was 0.16 wt.% SnO_2, or 0.3 mol%, which may be close to the equilibrium solubility of SnO_2 in In_2O_3 at this temperature.

An empirical formula for solvus boundaries can be developed on a thermodynamic basis using experimental solubility limits of SnO_2 in In_2O_3. Assuming ideal solution behaviour plotting $\ln X_{SnO_2}$ versus 1/T should create a straight line whose slope and intercept are $-\Delta H/R$ and $\Delta S/R$. ΔH is the enthalpy difference between SnO_2 in the bixbyite crystal structure and its equilibrium tetragonal form, while ΔS is the entropy difference for the same transformation. The data for the two-phase equilibrium region between In_2O_3 and SnO_2 given in Table 1 was used to create a plot of the type described, and is shown in Fig. 3. The experimental data used to create Fig. 3 shows that the ΔS and ΔH for the transition of SnO_2 into the bixbyite structure are 11.8 J/mol-K and 60,980 J/mol, respectively. These numbers indicate that SnO_2 has little affinity for the bixbyite structure. More importantly, the trendline in Fig. 3 can be extrapolated to determine the In_2O_3–SnO_2 solvus line at lower temperatures. The calculated solvus boundary using the trendline in Fig. 3 shows that the solubility limit of SnO_2 in In_2O_3 decreases rapidly and falls below 0.5 mol% between 900 °C and 800 °C [12].

The ability of In_2O_3 to incorporate substantial amounts of SnO_2 increases rapidly with increasing temperature despite the 13.75% difference between the atomic radii for In^{3+} and Sn^{4+} in coordination number (C.N.) VI (i.e., that of the bixbyite structure) [13]. In_2O_3 cationic sites can be derived from the fluorite structure by viewing this structure as having one fourth of the anionic sites vacant. The In_2O_3 lattice has a large interstitial site because of the oxygen vacancies inherent in the bixbyite structure, and the ability of the lattice to incorporate charge compensating oxygen interstitials required by the addition of Sn^{4+} may be linked to its relatively ''open'' defect-fluorite structure. Also, it has been shown that at high temperatures In_2O_3 becomes non-stoichiometric through the loss of oxygen [14]. Equation 1 illustrates this intrinsic defect mechanism.

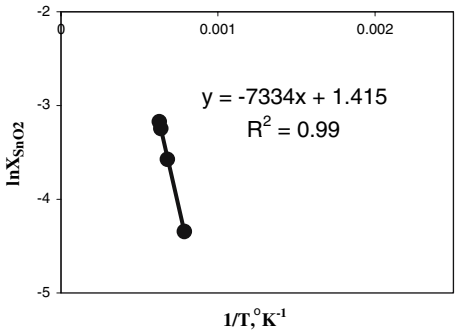

Fig. 3 Plot of $\ln X_{SnO_2}$ versus 1/T ($^\circ K^{-1}$), used to determine the empirical formula for the solvus boundary of SnO_2 in In_2O_3

$$In_2O_3 \rightarrow 2In_{In}^{x} + 2O_0^{x} + V_0^{\bullet\bullet} + 2e' \quad (1)$$

The intrinsic oxygen vacancy defect formation operative at elevated temperatures in In_2O_3 may aid the incorporation of SnO_2 into the lattice, in addition to the fact that the lattice has inherent oxygen vacancies with regard to the parent fluorite structure. As shown in Table 1, the maximum solubility of SnO_2 in In_2O_3 was found to be 13.1 mol% at 1650 °C. The large amount of SnO_2 that resides in the In_2O_3 lattice likely results in the formation of defect clusters or complexes, which have been the focus of early, and more recent studies [10, 15–18]. It appears that the temperature for the ultimate solubility limit of SnO_2 in In_2O_3 was not reached in this study, and based on these results, we believe that higher temperature (>1600–1650 °C) studies in this system are warranted.

The small amount of solubility of In_2O_3 in SnO_2 listed in Table 1 is expected when considering the crystal chemistry of the species involved. Crystalline SnO_2 has the rutile (TiO_2) crystal structure where the Sn^{4+} cations in C.N. VI have an atomic radius of 69 pm, while In^{3+} cations in C.N. VI have an atomic radius of 80 pm [13]. The In^{3+} is therefore not expected to have a large amount of substitutional solubility. Interstitial sites in the SnO_2 unit cell are certainly smaller than the ionic sites, so the interstitial mechanism of indium incorporation into the SnO_2 lattice is not favorable either. Similar observations regarding the small solubility of In_2O_3 in SnO_2 were found by Bates et al. [2], Edwards et al. [6], Frank et al. [7], but contrary results were reported by Enoki et al. [5].

The intermediate compound, $In_4Sn_3O_{12}$

$In_4Sn_3O_{12}$ has been determined to be isostructural with a large number of compounds that are referred to as M_7O_{12} compounds. Nadaud et al. [11] performed a detailed structural study of the compound. As with In_2O_3, the cationic sites in $In_4Sn_3O_{12}$ can be derived from the fluorite structure. $In_4Sn_3O_{12}$ formed quickly in these experiments. In_2O_3–SnO_2 mixtures were seen to form $In_4Sn_3O_{12}$ in three hours at 1350 °C and in less than 1 h at 1650 °C. Formation times were not studied in detail, but it is possible that they may have very fast reaction times, in the order of minutes. One reason for the swiftness of the reaction may be the similar ionic radii of indium and tin. It has been shown that systems with large differences in cation radii generally take longer to form the M_7O_{12} structure [19].

The experimental pattern for $In_4Sn_3O_{12}$ was indexed hexagonally and its lattice parameters were found to be a_h = 9.4628 (2) Å and c_h = 8.8563 (1) Å. The equivalent rhombohedral lattice parameters are a_r = 6.209Å and a = 99.27°. These lattice parameters are in close

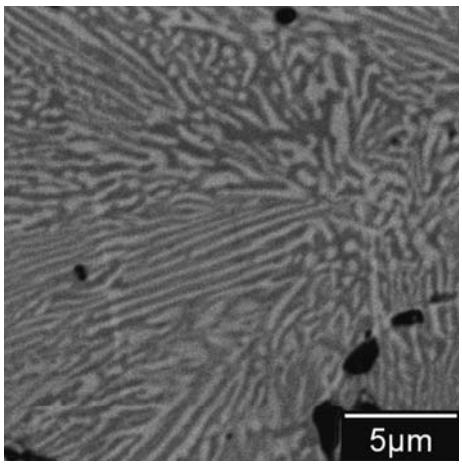

Fig. 4 Backscattered electron micrograph showing the lamellar structure that accompanied the eutectoidal decomposition of $In_4Sn_3O_{12}$ into In_2O_3 (light phase) and SnO_2 (dark phase)

agreement with those reported Bates et al. [2], and Nadaud et al. [11].

Figures 1 and 2 show that the $In_4Sn_3O_{12}$ phase is stable at temperatures above 1325 °C. XRD and microscopic examination showed that $In_4Sn_3O_{12}$ formed at 1350 °C and higher transforms eutectoidally into In_2O_3 and SnO_2 when sintered at temperatures of 1300 °C and below. The 1325 °C samples in this study were sintered for 45 h and no $In_4Sn_3O_{12}$ was observed using XRD and electron microscopy. Samples undergoing the eutectoid decomposition displayed the formation of an interesting lamellar microstructure, as shown in Fig. 4.

The intermediate compound, In_2SnO_5

The formation of a low temperature In_2SnO_5 phase through solid state sintering of In_2O_3 and SnO_2 was not obtained in this study. However, it was found that a phase with the stoichiometry In_2SnO_5 does form and is stable at elevated temperatures. Interestingly, the body color of In_2SnO_5 is yellow (similar to In_2O_3), however it is not quite as bright as pure In_2O_3. Figure 1 shows this phase to be a line compound. Close observation of the WDS data for this compound indicates that a small solid solution region may exist towards the indium oxide rich side, however the compound was not drawn as such because too few data points exist to make such a determination. Similar criteria as that applied to the $In_4Sn_3O_{12}$ phase were used in order to identify the eutectoidal decomposition temperature for In_2SnO_5. This phase was found to decompose eutectoidally into In_2O_3 and $In_4Sn_3O_{12}$ at temperatures below 1575 °C. The experimental XRD data for In_2SnO_5 is given in Table 2, and peaks with relative intensities of one or less have been omitted from the table for brevity. Efforts to

Table 2 Observed XRD data for In_2SnO_5

2θ	d_{meas}(Å)	$I/I_{o,meas}$	2θ	d_{meas}(Å)	$I/I_{o,meas}$
20.547	4.319	2	60.2405	1.5350	7
23.591	3.768	4	60.4664	1.5298	10
30.047	2.972	62	60.9424	1.5190	8
30.156	2.961	100	61.0200	1.5172	11
30.754	2.905	74	61.2148	1.5129	5
30.899	2.892	80	62.4570	1.4857	3
35.052	2.558	3	62.6846	1.4809	4
35.298	2.541	59	63.6245	1.4613	3
35.366	2.536	35	64.0415	1.4527	3
35.476	2.528	3	64.2954	1.4476	2
40.960	2.202	3	64.3861	1.4458	5
46.594	1.948	2	74.6397	1.2705	7
49.8619	1.8274	19	74.7997	1.2682	3
50.6554	1.8006	15	81.1321	1.1845	2
50.7584	1.7972	46	82.1027	1.1729	4
50.9420	1.7911	5	82.5112	1.1681	2
50.9997	1.7892	21	83.0805	1.1616	4
51.7632	1.7646	12	83.4116	1.1578	2
59.0465	1.5631	2	83.9279	1.1520	2
59.7310	1.5469	18	85.2927	1.1370	4
59.9390	1.5420	7	85.7343	1.1323	2
60.0627	1.5391	5	86.8987	1.1201	2

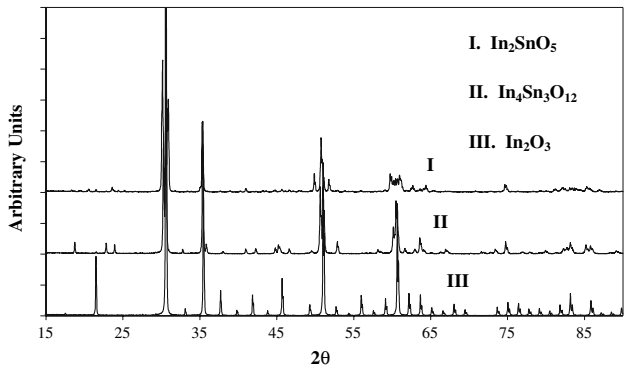

Fig. 5 Experimental x-ray diffraction patterns for In_2SnO_5, $In_4Sn_3O_{12}$, and In_2O_3

elucidate the crystal structure of In_2SnO_5 have been unsuccessful, however, because of similarities in the peak positions of the large intensity reflections of this phase with $In_4Sn_3O_{12}$ and In_2O_3, it is tempting to suggest that like those phases, In_2SnO_5 may be fluorite related in structure as well. In addition, it may be possible that In_2SnO_5 contains infinite ''strings'' of M[1]O_6 type polyhedra, like those known to exist in M_7O_{12} compounds and the bixbyite structure [10, 19–21]. The experimental patterns for these three phases are given in Fig. 5, and it can be seen that considerable overlap exists between the large intensity peaks.

The report of this phase should prompt further investigation into the bulk and thin film properties of this compound, particularly in light of the high SnO_2 content in In_2SnO_5 and increased study of ternary compounds as starting materials for deposition of transparent conductors [22–24]. This compound is attractive as a possible alternative material for ITO because of its lower cost resulting from the high tin content.

Conclusions

This study has produced the most complete In_2O_3–SnO_2 phase diagram to date. The solvus boundary of In_2O_3 with SnO_2 indicates that most commercial SnO_2-doped In_2O_3 thin films are thermodynamically metastable, and substantially supersaturated with SnO_2. This fact also suggests that the two line compounds, $In_4Sn_3O_{12}$ and In_2SnO_5, found in the phase equilibria of In_2O_3–SnO_2, may also be stabilized at the low processing temperatures used in the production of ITO thin films. We have also shown evidence of the In_2SnO_5 phase for the first time, which decomposes eutectoidally at 1575 °C. This phase may prove to be an attractive composition to explore as a novel transparent conducting oxide.

Acknowledgements The primary author would like to thank Dr. S. M. Loureiro (GEGR) for careful review of the manuscript. In addition, O. Mills (electron microscopy and EMPA), E. Laitila (XRD), and R. Kramer (metallography) of Mich. Tech. Univ. are given thanks for assistance in materials characterization.

References

1. Lewis BG, Paine DC (2000) MRS Bulletin 25(8):22
2. Bates JL, Gritten CW, Marchant DD, Garnier JE (1986) Am Ceram Soc Bull 65:673
3. Solov'eva AE, Zhdanov VA (1985) Inorg Mater 26(6):828
4. Varfolomeev MB, Mironova AS, Chibirova FKh, Plyushchev VE (1975) Inorg Mater (Eng Transl.) 11(12):1926
5. Enoki H, Echigoya J, Suto H (1991) J Mater Sci 26:4110
6. Edwards DD, Mason TO (1998) J Am Ceram Soc 81:3285
7. Frank G, Brock L, Bausen HD (1976) J Crystal Growth 36:179
8. Ohya Y, Ito T, Kaneko M, Ban T, Takahashi Y (2000) J Ceram Soc Japan 108:803
9. Kanai Y (1984) Jap J App Phys 23(1):L12
10. González GB, Mason TO, Quintanta JP, Warschkow O, Ellis DE, Hwang J-H, Hodges JP, Jorgensen JD (2004) J App Phys 96(7):3912
11. Nadaud N, Lequeux N, Nanot M, Jové J, Roisnel T (1998) J Solid State Chem 135:140
12. Heward WJ (2002) M.S. Thesis, Investigation of Phase Equilibria in In_2O_3-Based Binary Systems for use in Transparent Conducting Oxide Applications, Michigan Technological University
13. Dean JA (1992) Lange's Handbook of Chemistry, 14th edn. McGraw-Hill, Inc. NY, 4.13. Refers to Shannon RD, Prewitt CT (1969) Acta Cryst., B25:925 and Shannon RD (1976). Acta Cryst. A32:751
14. De Wit JHW (1977) J Solid State Chem 20:143
15. Frank G, Köstlin H (1982) Appl Phys A: Mater Sci Process 27:197
16. Warschkow O, Ellis DE, González GB, Mason TO (2003) J Am Ceram Soc 86(10):1700
17. Warschkow O, Ellis DE, González GB, Mason TO (2003) J Am Ceram Soc 86(10):1707
18. González GB, Cohen JB, Hwang J-H, Mason TO, Hodges JP, Jorgenson JD (2001) J App Phys 89(5):2550
19. Rossell HJ (1976) J Solid State Chem 19(2):103
20. Ray SP, Cox DE (1975) J Solid State Chem 15:333
21. Ray SP, Stubican VS (1977) Mater Res Bull 12:549
22. Minami T (2000) MRS Bulletin 25(8):38
23. Freeman AJ, Poeppelmeier KR, Mason TO, Chang RPH, Marks TJ (2000) MRS Bulletin 25(8):45
24. Edwards DD, Mason TO, Goutenoire F, Poeppelmeier KR (1997) Appl Phys Lett 64:2071